

Thermal-Structural Plasma Gouging Simulation for Welding Repair

Douglas S. M. Serrati¹ , Douglas B. Araújo¹ , Louriel O. Vilarinho¹ 

¹ Universidade Federal de Uberlândia, Faculdade de Engenharia Mecânica, Uberlândia, MG, Brasil.

How to cite: Serrati DSM, Araújo DB, Vilarinho LO. Thermal-structural plasma gouging simulation for welding repair. *Soldagem & Inspeção*. 2023;28:e2807. <https://doi.org/10.1590/0104-9224/SI28.07>

Abstract: Numerical simulations are commonly employed for comprehending and prognosticating welding procedures. However, repair often requires supplementary actions such as gouging for defect removal. Thermal cycles and non-uniform expansion and contraction of the base metal can engender internal and residual stresses in the gouged region. Residual stresses can wield influence over mechanical properties, thereby underscoring the necessity for their investigation. This study endeavors to establish a numerical method to simulate gouging while devising a rationale for thermal cutting processes. The model was validated by comparing computational and experimental results, which showed good agreement. Mechanical simulation unveiled residual stresses characterized by modest magnitude. This methodology can prevent mechanical failures in repaired components by providing valuable insights into the effects of the gouging process.

Key-words: Simulations; Residual stress; Weld; Repair; Gouge; Numerical study.

1. Introduction

Gouging is a thermal cutting process that melts metal to remove weld beads or create bevels for subsequent weld filling. Due to the removal of material through heat, a large amount of energy is used, resulting in significant temperature variations. As a result, residual stresses and distortions can occur in the gouged part, which can ultimately affect the mechanical strength and function of the welded part or structure.

Residual stresses are defined as the stresses present in a welded joint or base metal that is free of external stresses and thermal gradients [1], which is in agreement with the definitions of American Welding Society [2]. The stresses that initiate during welding and cooling can also be classified as part of the residuals by some authors [3]. These stresses can have a significant influence on the mechanical strength and function of the welded part or structure, and can contribute to its early failure.

The residual welding stresses can originate from several factors, including intense surface cooling, contraction during cooling of differently heated and plasticized regions during welding, and phase transformations [4]. Additionally, other operational factors can influence the intensity of these residual stresses.

Despite attempts to define and quantify the separate effects of each operational factor on the generation of residual stresses through computational or experimental analysis, the literature presents conflicting results [5]. Additionally, distortion or collapse can occur in a welded structure that lacks sufficient stiffness to relieve residual stresses [6].

One potential issue with gouging is microstructural transformations in the material due to multiple thermal cycles resulting from welding, gouging, and re-welding. Previous experimental work [7-9] has examined the effects of such repairs on the mechanical and microstructural properties of different materials.

While numerous thermal and mechanical simulations of welding processes exist, few studies address gouging simulations. However, some works [10-12] have simulated the laser cutting process, which, in some extent, is close to the computational approach for gouging simulation.

The relationship between the welding and gouging processes, coupled with the different directions in the scientific advances of each, suggests that gouging simulations are more complex than welding simulations. In a recent study [13], a thermal simulation of gouging was developed, but to simplify the physical phenomena and reduce the complexity of the numerical study, the dimensions of the section that would be removed by melting were modeled. This limits the applicability of the results in practice.

To address these issues, this study aims to model the entire assembly without controlling the dimensions of the gouged region, which will be obtained through simulation. Furthermore, the study aims to determine the arrangement and intensity of the residual stresses that occur during gouging processes, which are not yet well understood. By avoiding simplifications that can manipulate results and making gouging simulations more reliable, this study aims to contribute to a better understanding of gouging and its effects on welded structures.

Received: 11 May, 2023; Accepted: 10 Oct., 2023.

*E-mails: douglasserrati@gmail.com (DSMS), dbaraujo@ufu.br (DBA)



This is an Open Access article distributed under the terms of the [Creative Commons Attribution license](https://creativecommons.org/licenses/by/4.0/), which permits unrestricted use, distribution, and reproduction in any medium, provided the original work is properly cited.

2. Experimental Procedure

The experimental procedure was carried out in order to calibrate and validate the numerical model. The experiments involved plasma gouging of a 400 x 300 x 25.4 mm structural steel plate (ASTM A131 EH36), using a Computer Numerical Control (CNC) table. The gouging process was performed utilizing an air pressure of 55 psi, an electric current of 60 A, a voltage of 215 V, a torch travel speed of 5.1 mm/s, a contact-to-work distance of 15 mm, and a torch travel angle of 45°.

To improve the accuracy of the measurements, a portion of the gouged region was scanned using a Creaform HandySCAN307 3D laser scanner, with 0.1 mm resolution. An imaging processing software (VXelements and VXmodels) was used to analyze the results. Additionally, a part of the gouged region was crosswise cut and analyzed via macrograph to identify the Heat-Affected Zone (HAZ) region. The experimental results used for numerical model calibration included the width, depth, and transverse contour of the material withdrawal region, as well as the dimensions of the HAZ.

3. Simulation Model

The software Ansys Multiphysics APDL (Ansys Parametric Design Language) was used for all stages of the numerical study.

The present study commences with the preparation of the thermal and mechanical simulation model, which involves the design and meshing of the gouged plate. To achieve symmetry in the case study, the gouging is carried out along the plate's centerline. Consequently, it becomes feasible to simplify the simulation model by modeling only one-half of the gouged plate. The simulation's temperature distribution is perfectly symmetrical, since it is a simulation.

The mesh size utilized in the gouging region was 0.2 mm, whereas the size of the mesh in the farthest regions of the plate's center was 2 mm. The total number of nodes within the mesh was 386,131. The mesh employed within the gouging and farthest regions from it were of the structured type, with a transition between these regions using an unstructured mesh. This can be observed in Figure 1a. Also, the symmetry is used in the locking scheme for the mechanical simulation, which is shown in Figure 1b. The perspective of the plate has been altered in relation to Figure 1a in order to facilitate the visualization of the locking points. In Figure 1b can be observed that the brown face is completely prevented from moving in the direction of the x-axis, due to the simulated model being symmetric and the brown face being the plane of symmetry.

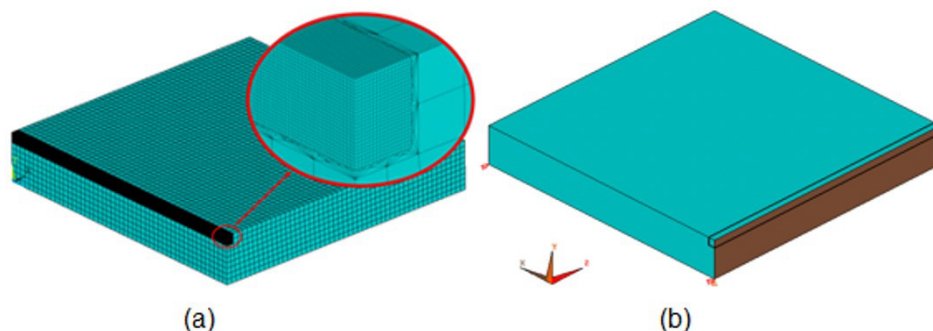


Figure 1. Gouging simulation mesh (a) plate fixing for mechanical simulation (b)

It should be noted that each type of simulation requires a specific kind of element, designated to calculate either temperature or stress and distortion.

During the thermal analysis, the SOLID70 element with 8 nodes and 1 degree of freedom per node was utilized to account for conduction and convection heat transfer. In addition, the SURF152 element was employed to apply the radiation heat transfer condition on the entire part's outer surface.

In contrast to the thermal simulations, the mesh utilized in the mechanical simulations remained constant. However, the element type was modified to SOLID185, which is geometrically comparable to SOLID70. SOLID185 was implemented to calculate stress and distortion within the material.

Despite being low-order elements, refining them in the region with the highest thermal gradient within the mesh yields favorable outcomes [14-17].

4. Thermal and Mechanical Numerical Analysis

The second step in this study involves conducting a thermal simulation to identify the HAZ and the dimensions of the gouged section. To achieve this, a set of equations are solved through iterative computation during the simulation process. It is essential to define the thermally dependent properties of the material and the heat source used for energy imposition to obtain accurate simulation results.

The temperature field in the numerical model is governed by the heat conduction equation given by Equation 1.

$$\rho(T)C_p(T)\frac{\partial T}{\partial t} = \frac{\partial}{\partial x}\left(k(T)\frac{\partial T}{\partial x}\right) + \frac{\partial}{\partial y}\left(k(T)\frac{\partial T}{\partial y}\right) + \frac{\partial}{\partial z}\left(k(T)\frac{\partial T}{\partial z}\right) + Q_v \quad (1)$$

In this study, T is temperature, $k(T)$ is the thermal conductivity of the temperature-dependent material, $\rho(T)$ is the specific mass of the material, $C_p(T)$ is specific heat, and Q_v is the energy generated per unit of volume (in this study, Q_v is null).

The thermodynamic boundary conditions applied were convection and radiation, both applied to the external surfaces of the material. Convection heat flow (q_c) in a medium with gas or liquid is given by Equation 2 of Newton's heat transfer law.

$$q_c = h_c(T - T_0) \quad (2)$$

The temperature of the outer surface of an object is denoted by T , while T_0 represents the temperature of the gas or liquid surrounding the object. The coefficient of heat transfer by convection is represented by h_c . In the literature, various values for the convection coefficient have been proposed, with some authors [18-20] suggesting a value between 5 to 20 W/m²K.

The heat flow by radiation (q_r) is governed by Equation 3 of Stefan-Boltzmann's law.

$$q_r = \varepsilon_r \sigma_r (T^4 - T_0^4) \quad (3)$$

The emissivity value of a material's surface is denoted by ε_r , while the Stefan-Boltzmann constant is represented by σ_r , equal to 5.67×10^{-8} Wm⁻²K⁻⁴. The value of emissivity is dependent on the condition and temperature of the material's surface.

The source under analysis is a modification of the Gaussian source, known as the modified three-dimensional (MTD) source, which varies its radius logarithmically along the Z axis (i.e., along the thickness of the plate). This type of heat source was demonstrated by Dhinakaran et al. [21]. Equations 4 to 7 presents the mathematical model of MTD, while

$$Q(r, z) = Q_0 \exp\left(-\frac{3r^2}{r_0^2}\right) \quad (4)$$

$$r_0(z) = a \ln(z) + b \quad (5)$$

$$a = \frac{r_e - r_i}{\ln(z_e) - \ln(z_i)} \quad (6)$$

$$b = \frac{r_i \ln(z_e) - r_e \ln(z_i)}{\ln(z_e) - \ln(z_i)} \quad (7)$$

The function $Q(r, z)$ represents the distribution of heat flow in the volume, which depends on both the radial and depth coordinates of the source. Q_0 , on the other hand, refers to the total imposed heat, which is calculated as the product of the power and efficiency of the process. The upper radius of the source is represented by r_e , while the lower radius is represented by r_i . Z_e and Z_i denote the starting and ending positions of the source, respectively, in the z direction.

For the thermal simulation, a convection coefficient of 15 W/m²K [1,3] was defined at a room temperature of 25 °C. To model the emissivity of the material, a value of 0.80 was utilized [3]. The arc efficiency was set to 0.85 [1,3].

The third step in this study was the mechanical simulation. With the aim of calculating residual stresses and distortions from the gouging process, it is necessary to perform thermal-structural coupling. This involves utilizing the results from the thermal analysis, which provide a history of temperature distribution at each instance, and accepting them as forces in the structural simulation (i.e., expansion and compression).

For the numerical structural analysis of the welding process, the total deformation that occurs during the process is decomposed into three components, as shown in Equation 8.

$$\varepsilon_t = \varepsilon^e + \varepsilon^p + \varepsilon^t \quad (8)$$

Where ε_t represents the total deformation calculated by elastic deformation (ε^e), which is modeled using Hooke's law, the modulus of elasticity (E) and Poisson's ratio (ν). Regarding plastic deformation (ε^p), a plasticity model is employed with the material's yield strength (σ). And the thermal deformation (ε^t) is calculated using the material's coefficient of thermal expansion (α). From this information, deformations in the plates, as well as residual stresses, are calculated.

Additionally, other thermally dependent thermal and mechanical properties based on previous studies [22] for ASTM A131 steel can be found in Table 1. The properties vary linearly between the temperatures specified in Table 1, which Ansys APDL will automatically define the remaining properties values through linear interpolation. The temperature values defined in Table 1 are based on the linear changes in the properties' graphical behavior [22].

Table 1. Mechanical and thermal properties thermally dependent of ASTM A131 steel.

Mechanical properties				
T [°C]	σ [MPa]	E [GPa]	α [$10^{-6}/K$]	ν
25	343.0	205.3	12.1	0.3
375	245.5	173.5	12.6	0.36
450	210.6	130.6	12.8	0.38
525	172.0	89.4	12.8	0.39
600	127.5	60.0	12.8	0.4
750	67.4	35.3	13.1	0.43
975	20.5	12.9	13.4	0.48
1050	12.0	10.6	13.6	0.48
1400	12.0	10.6	13.6	0.48
Thermal properties				
T [°C]	ρ [kg/m^3]	k [W/mK]	Cp [J/kg°C]	
0	7774.4	54.9	385.0	
700	7618.2	30.6	893.7	
744	7600.9	29.0	1230.9	
800	7583.5	25.2	913.3	
900	7566.2	26.2	621.1	
1400	7444.7	30.5	795.3	

Another need for mechanical simulation is to constrain the gouged plate. This was done in a way that leaves it as free as possible, in order to only constrain it to ensure it does not move along the axes when thermal loads are applied. The plate is free to deform as shown in Figure 1b.

5. Gouging Numerical Procedure

In numerical simulations of gouging or welding processes, heat is often introduced using heat sources. In the present study, the MTD heat source was employed to impose a heat flow on the mesh nodes at each time step (i.e., in each time interval Δt). The value of Δt used for heat application was calculated based on the travel speed of the welding or gouging process (v) and the size of the elements (d_n), as shown in Equation 9.

$$\Delta t = \frac{\Delta S}{v} = \frac{d_n}{v} \quad (9)$$

In this context, the symbol Δt represents the duration of heat source exposure at each node in the current steps. ΔS denotes the change in space (which refers to the distance between two points). The symbol v represents the gouging travel speed, while d_n is the distance between the nodes.

In the present work, the gouging process was simulated using algorithms similar to those employed in welding processes. However, in addition to the traditional thermal solution, the material melted by the heat source was made to disappear using the “birth and death” technique. This technique involves not only the appearance or disappearance of elements, but also the change in properties of the mesh. Specifically, the stiffness matrix of the finite element technique receives a very small value, typically 10^{-6} in the case of Ansys software, which is used in this study. For heat transfer problems, the stiffness matrix is related to thermal conductivity.

In the present investigation, the “death” condition of the elements is defined as the melting temperature of the material, that is $1450^\circ C$ for steel. However, this type of analysis is not straightforward, as the temperature needs to be determined at each step of the simulation. This requires the algorithm to exit the solution at each step and enter post-processing mode to monitor the temperature throughout the mesh before resuming the analysis. Additionally, since the region where the heat source is applied reaches very high temperatures, it becomes deactivated and cannot continue to apply heat to dead elements. Since the conductivity is practically zero, the temperature would rise to very high levels. To circumvent this issue, the region of the next heat application is reactivated. The complete process is described in the following sequence:

- (1) Nodes where heat source is to be applied are selected;
- (2) Elements associated with these nodes are saved to an external file;
- (3) Heat is applied to the nodes using the heat source equation (Eq. 4) and a given time interval (Eq. 9);
- (4) The solution is exited and post-processing is performed to obtain the temperature distribution throughout the mesh;
- (5) Elements that reach temperatures above $1450^\circ C$ are identified;
- (6) These elements are saved to another external file;
- (7) The EKILL control is used to deactivate elements that exceeded the temperature limit;
- (8) The function ANTYPE “restart” is applied to recalculate the solution with the dead elements;
- (9) Heat source elements saved in step 2 are reactivated using the EALIVE command;
- (10) The heat source is moved to the front nodes in the direction of gouging;
- (11) The process resumed from step 1.

In summary, by employing the “birth and death” technique for finite element analysis, were possible to simulate the gouging process and incorporate the disappearance of the melted material. Although the analysis was complicated due to temperature monitoring and the deactivation of the heat source region, was necessary to revive the next heat application region to address the high temperature issue.

Thus, when continuing a numerical study from thermal to mechanical, it is necessary to interpret the temperature distribution at each time step of the gouging process and subsequently inform the software which elements should be deactivated at that step. For this reason, the mechanical solution of the gouging process is not trivial, as it requires knowledge of, when and which, elements have reached the melting temperature in the previously conducted thermal numerical study.

Therefore, the complete sequence of the mechanical simulation process in gouging is described below:

- (1) The temperature distribution results obtained from the thermal simulation at the current step are read;
- (2) The file in which the elements that reached the material's melting temperature in the thermal simulation were identified and saved, is read;
- (3) The identified elements are deactivated using the “birth and death” technique;
- (4) Calculations are performed for these imposed conditions;
- (5) The process is resumed from item 1.

Figure 2a presents a flowchart comparison between the solution of a thermal simulation of welding (a-left) and gouging (a-right) processes, utilized in the current study. Where E_{melt} is the name of the file in which the elements to be removed are stored. While the parameters $T_{elements}$ and T_{melt} are the temperatures of the elements and the melting temperature of the steel, respectively.

The methodology of the mechanical numerical study is simpler as it leverages data previously obtained in the thermal simulation solution process. Figure 2b shows a flowchart comparison between the mechanical simulation solution of the welding (b-left) and gouging (b-right) processes used in this work.

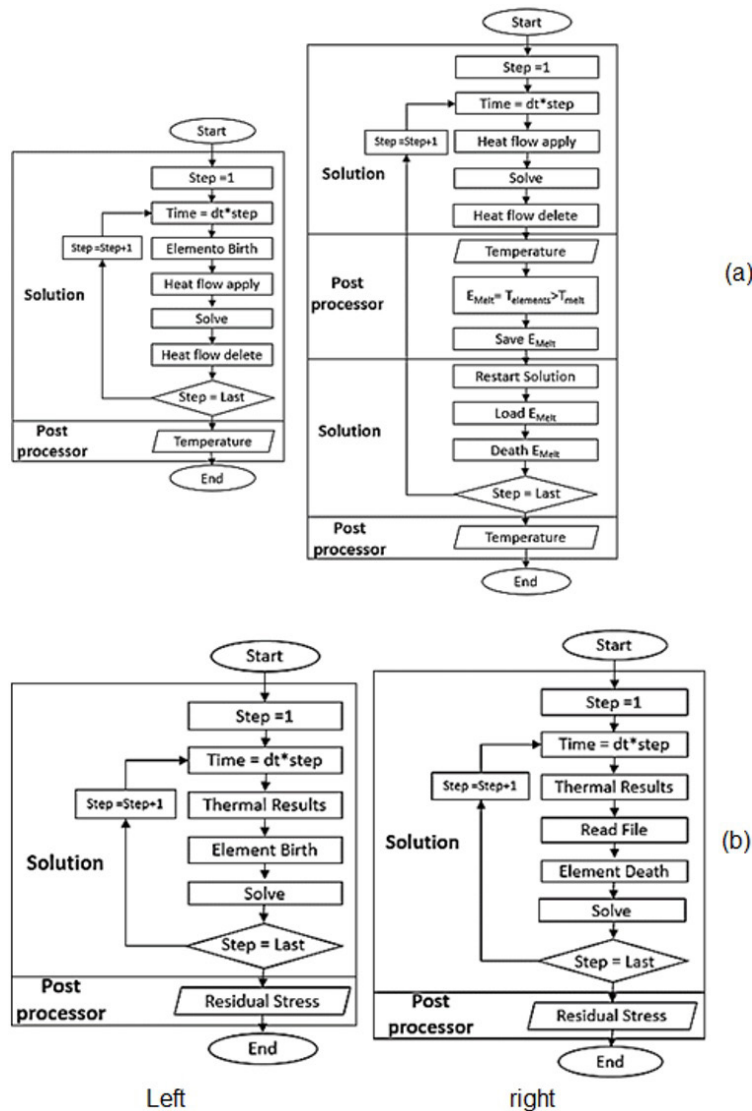


Figure 2. Flow diagram sequential of thermal numerical welding (a-left) and gouging (a-right) processes, and the flow diagram sequential of mechanical numerical welding (b-left) and gouging (b-right) processes.

6. Results and Discussion

Initially, macrography of the gouged cross-sectional area was conducted, with a sample taken 25 mm from the end of the gouging. This sample is presented in Figure 3a and is used to validate the computational simulation by comparing the width and depth of the removed material section and the heat-affected zone as shown in Figure 3b.

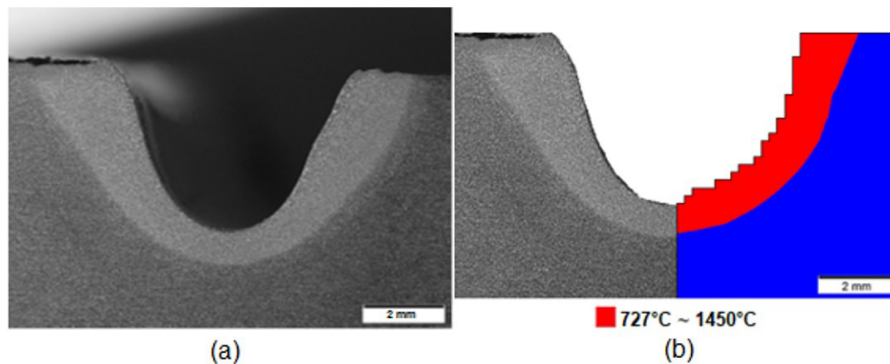


Figure 3. Macrography of the gouged cross-sectional area (a) and comparison between experimental and numerical cross section and heat affected zone (b).

To determine the dimensions of the gouged section, a 3D scanning of the metallographic sample was performed. Regarding depth, the highest depth measurement was adopted as it showed uniformity throughout the sample, as observed in the color map in Figure 4a, with a value of 4.34 mm. The gouged width showed variations along the length of the gouge. Therefore, measurements were taken in ten sections along the gouge, and an average value of 6.20 mm was adopted, as presented in Figure 4b.

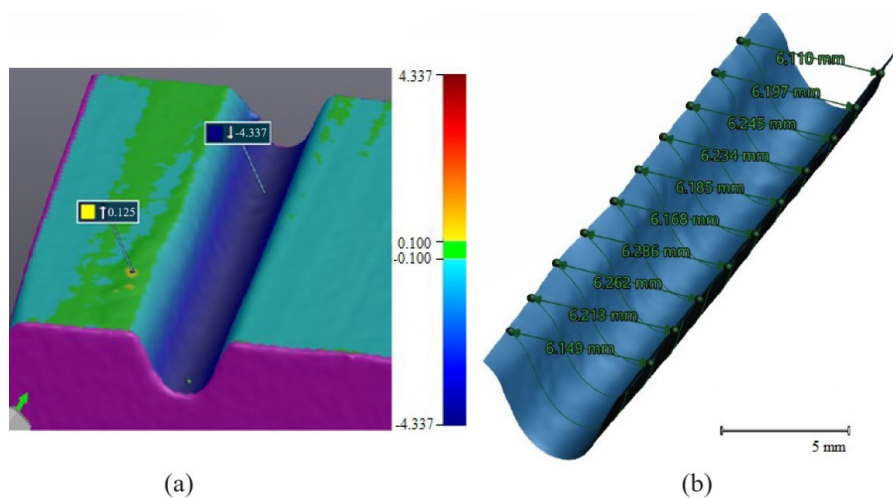


Figure 4. Measurement of the depth (a) and width (b) of the gouged section by 3D scanning.

By observing Figure 4, it is possible to verify that both the depth and width of the material removal by the gouging process do not have a very pronounced variation along the analyzed length. Therefore, the material removal process occurred in a uniform and stable manner along the length of the plate.

With the experimental procedure finished, the study conducted a comparison between the results obtained from experimental and numerical gouging. It was found that the experimental and numerical model exhibited similar results, as depicted in the cross-sectional gouging and heat affected zone image presented in Figure 3b.

It is noteworthy that the discernible “steps” exhibited in the simulation outcomes presented in Figure 3b are attributable to the mesh. In the course of the simulation, the software determined the region that underwent gouging and subsequently removed the elements with temperatures exceeding the material's melting temperature, leaving the adjacent elements intact. This constitutes the methodology adopted in this study, differing from the approach presented in reference [13]. In [13], the parameters relating to the width and depth of the gouged section are treated as input parameters, meaning they are predetermined. In contrast, this study acknowledges that, akin to real-world scenarios, the values of width and depth are initially unknown, thus regarding them as output parameters in this context. This outcome yields the observed visualization in the form

of “steps”. It is anticipated that the refinement of the gouging volume mesh will progressively reduce the “step-like” visual effects, leading to a closer resemblance to the experimental results.

The experimental measurements of the depth and width were 4.34 mm and 6.20 mm, respectively. While for numerical calculations, it were 4.40 mm and 6.40 mm, respectively.

In order to obtain the results, the heat source parameters as defined by Equations 4 through 7 were established at values of 3, 3.7, 0.1, and 4 mm for the variables r_e , r_i , Z_e and Z_i , respectively. The visual representation of the heat source is depicted in Figure 5a, through a perspective view of the complete model which has been mirrored in the plane of symmetry. Meanwhile, Figure 5b illustrates the heat source at the same moment in time, but in a cross-sectional view along the axis of symmetry.

Based on the analysis of Figure 5, it can be inferred that the appearance of the heat source aligns with the anticipated outcomes derived from the mathematical calculations conducted according to Equations 4 to 7.

Through experimental validation, it can be inferred that the mechanical simulation results are accurate. This is because the validated numerical thermal study results are employed in the mechanical simulation. Additionally, the mechanical properties have been correctly established [22], and the clamping of the sheet is executed in the same manner as it is in the experiment. Hence, there is sufficient foundation to consider the mechanical simulation results as valid.

There is no literature available that describes the intensity or arrangement of residual stresses generated during the gouging process. Given that, residual stresses on the top surface of the sheet were analyzed.

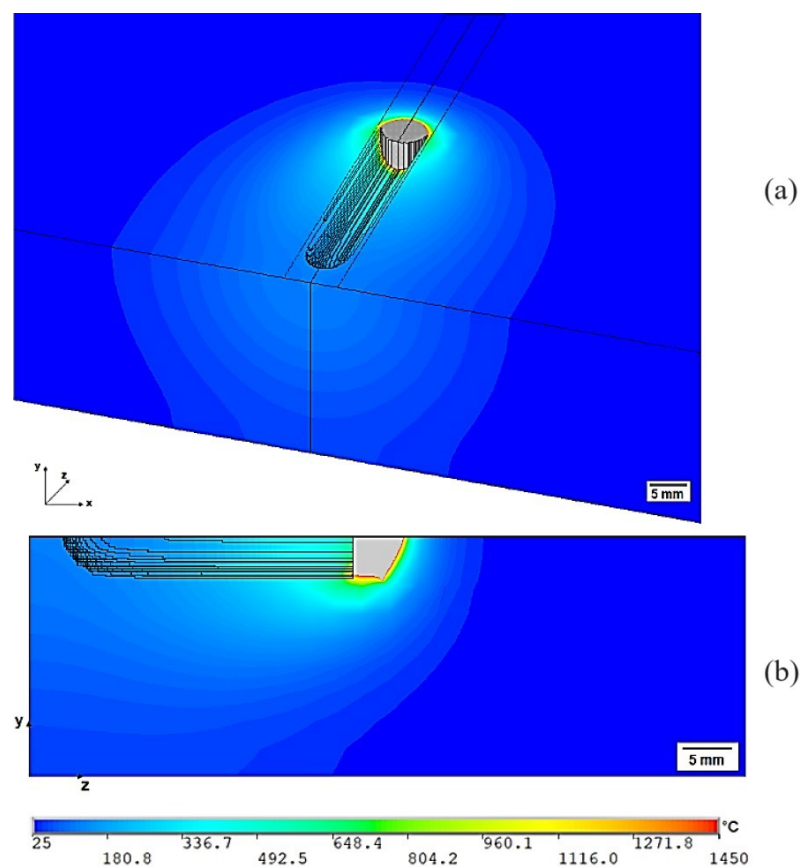


Figure 5. Thermal field of gouging with expanded symmetry (a) and in the plane of symmetry (b).

Initially, stress results were obtained to provide a general perspective on the intensity and arrangement of the stresses. Longitudinal and transverse residual stresses in relation to the gouged length were analyzed in a manner analogous to that employed in works on welding process simulations. Figure 6 illustrate the arrangement of longitudinal (a) and transversal (b) residual stresses in the gouged sheet. Subsequently, graphs are presented that facilitate a more objective analysis of these stresses.

In order to create charts of the top surface of the plate, longitudinal stresses were obtained along the center of the gouged region and parallel to its side (at a distance of 4.5 mm). The transverse stresses are those present transversely to the direction of gouging at half the length of the plate.

First, the longitudinal residual stress in the center of the gouged section and adjacent to it is analyzed on the top surface. Both stress distribution curves are presented in Figure 7. The transversal residual stress on the upper surface is also illustrated in Figure 7c.

It is observed that in Figure 7a, the beginning and end of the plate length present marked stress variations, due to irregularities generated in the mesh at the start and end of the process, which are moments of transient regiment of the heat source. These

irregularities can be observed in Figure 5. On the other hand, in Figure 7b, greater stability of residual stresses is verified, which is justified by the complete presence of all mesh elements and by being located in a non-critical location during the process.

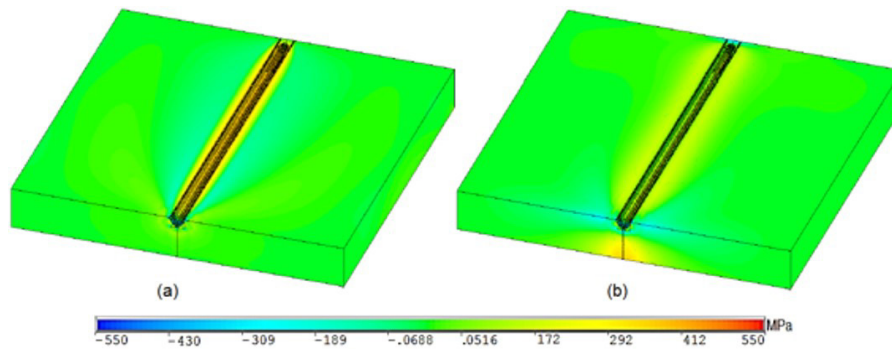


Figure 6. Perspective view of the gouged plate with display of the longitudinal (a) and transversal (b) residual stress distribution.

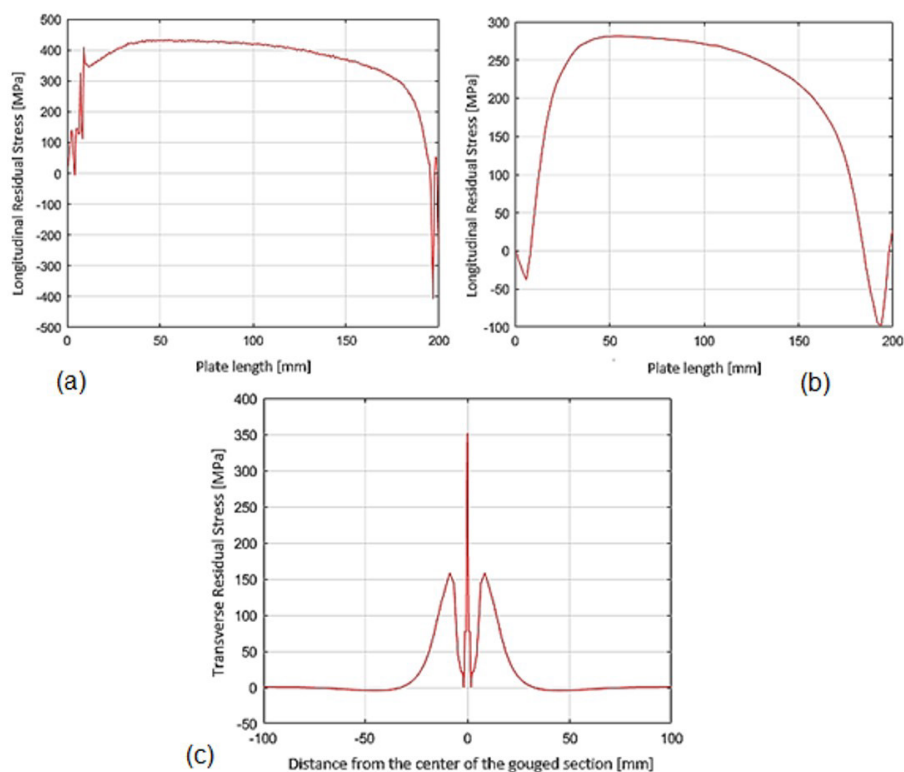


Figure 7. Longitudinal residual stress in the center of gouged region (a), longitudinal residual stress beside the gouged region (at a distance of 4.5 mm from the center) (b) and transversal residual stress on the upper surface (c).

The disposition of transverse stress on the upper surface in Figure 7c has been previously described in a welding study [23]. Unlike welding, where filler metal is deposited, in gouging, the melted base metal is removed. Therefore, the highest tensile stresses are observed at the center of the gouged region since this section undergoes the most heating, and its tensile strength is reduced when heated, according to the material's Table 1 properties. Similarly to the study [23], in the heat-affected zone, the reduction of transverse residual stress to zero is attributed to the numerical study. Since the gouged dimensions were not considered as input parameters, as in the manner of [13], the removal of mesh elements to create the “step-like” visual effect shown in Figure 3b necessitates that nodes belonging to the adjacent elements of those removed (and shared with them) possess a null residual stress value. This is due to their preservation of equilibrium conditions and susceptibility to greater distortions. After the heat-affected zone, the stresses become tensile again.

7. Conclusion

Based on the presented results, it can be concluded that the simulation method developed using a MTD heat source was able to provide results that closely match the experimental data, without any manual adjustment of the width or depth of the material removal resulting from gouging.

In general, gouging tends to result in lower residual stresses. This is due to the removal of heated material during the process, leading to reduced intensity of thermal cycles experienced by the underlying base metal. The diminished dissipation of energy in the gouged plate contributes to this effect. Figure 7c illustrates that the transverse residual stress reaches its maximum at the center of the gouged area, gradually diminishing to zero upon entering the heat affected zone. It subsequently increases, then decreases along the base metal. Meanwhile, the longitudinal residual stress exhibits transient behavior at the outset and conclusion of the gouging process, corresponding to the initiation, stabilization, and termination of the electric arc, as depicted in Figure 7a.

With respect to distortions, it can be concluded that they occur with higher intensity in the transient regime of the heat source. Despite the plate being clamped only to the minimum required, it exhibited low levels of distortion, which can be attributed to the fact that the heated material is removed in the gouging process. By eliminating elements with high temperature, the temperature is not conducted intensively to the remaining base metal, and due to the low thermal cycle, small distortions are obtained. It is important to note that the gouged plate is thick and of small dimensions, which also contributes to the reduction of distortion levels.

Disclosure statement

The authors declare that they have no conflict of interest.

Funding

This research is supported by Petrobras, ANP, CAPES, CNPq, and FAPEMIG.

Statements and declarations

The data and code that support the findings of this study are available from the corresponding author, upon reasonable request. All authors have read and agreed to the published version of the manuscript.

Authors' contributions

DBA and LOV: conceptualization and methodology. DSMS and DBA: simulation, data accuration and 3D scanning. DSMS: writing - original draft preparation. LOV and DBA: writing - revision.

References

- [1] Serrati DSM. Numerical simulation of plasma gouge process [masters dissertation]. Uberlandia: Federal University of Uberlandia; 2022. <http://doi.org/10.14393/ufu.di.2021.684>
- [2] American Welding Society. AWS A3.0M/A3.0:2010: standard welding terms and definition. 12th ed. Miami: AWS; 2010. 162 p.
- [3] Araújo DB. Study of distortion in welding by using numerical and optimization techniques [doctor thesis]. Uberlandia: Federal University of Uberlandia; 2012.
- [4] Macherauch E. Different sources of residual stress as a result of welding. In: Residual Stress in Welded Construction and their Effects: An International Conference; Nov 15-17; London. Cambridge: Welding Institute; 1977. p. 267-282.
- [5] Mishchenko A, Scotti A. Tensões residuais em soldagem a arco: uma visão holística. Soldagem e Inspeção. 2018;23(1):93-112. <http://dx.doi.org/10.1590/0104-9224/si2301.10>.
- [6] Gurova T, Quaranta F, Estefen S. Monitoramento do estado das tensões residuais durante fabricação de navios. In: 21º Congresso Nacional de Transporte Aquaviário, Construção Naval e Offshore; Rio de Janeiro. Rio de Janeiro: SOBENA; 2006.
- [7] Lin CM, Tsai HL, Cheng CD, Yang C. Effect of repeated weld-repairs on microstructure, texture, impact properties and corrosion properties of 304L stainless steel. Engineering Failure Analysis. 2012;21:9-20. <http://dx.doi.org/10.1016/j.engfailanal.2011.11.014>.
- [8] Vega OE, Hallen JM, Villagomez A, Contreras A. Effect of multiples repairs in girth welds of pipelines on the mechanical properties. Materials Characterization. 2008;59(10):1498-1507. <http://dx.doi.org/10.1016/j.matchar.2008.01.011>.
- [9] Aghaali I, Farzam M, Golozar MA, Danaee I. The effect of repeated repair welding on mechanical and corrosion properties of stainless steel 316L. Materials & Design. 2014;54:331-341. <http://dx.doi.org/10.1016/j.matdes.2013.08.052>.
- [10] Fu CH, Sealy MP, Guo YB, Wei XT. Finite elements simulation and experimental validation of pulsed laser cutting of nitirol. Journal of Manufacturing Processes. 2015;19:81-86. <http://dx.doi.org/10.1016/j.jmapro.2015.06.005>.
- [11] Kheloufi K, Amara EH, Benzaoui A. Numerical simulation of transient three-dimensional temperature and kerf formation in laser fusion cutting. Journal of Heat Transfer. 2015;137(11):112101. <http://dx.doi.org/10.1115/1.4030658>.
- [12] Saternus Z, Piekarska W, Kubiak M, Domanski T, Kroliszewska DG. Numerical modeling of cutting process of steel sheets using a laser beam. In: MATEC Web of Conferences. Les Ulis: EDP Sciences. Vol. 254, p. 08004. <http://dx.doi.org/10.1051/mateconf/201925408004>

- [13] Hyun C, Bae K, Yi M. A study on heat flow and thermal distortion in terms of air-carbon-arc gouging of steel plates. *Proceedings of the Institution of Mechanical Engineers. Part B, Journal of Engineering Manufacture*. 2018;232(12):2210-2217. <http://dx.doi.org/10.1177/0954405416685385>.
- [14] Akella MS, Harinadh MV, Krishna MY, Buddu MRK. A welding simulation of dissimilar materials SS304 and copper. *Procedia Materials Science*. 2014;5:2440-2449. <http://dx.doi.org/10.1016/j.mspro.2014.07.490>.
- [15] Bai RX, Guo ZF, Lei ZK. Prediction of welding deformation and residual stress of stiffened plates based on experiments. In: *IOP Conference Series: Materials Science and Engineering*. Bristol: IOP Publishing; 2017. p. 012032. <http://dx.doi.org/10.1088/1757-899X/281/1/012032>.
- [16] Del Coz Díaz JJ, Menéndez Rodríguez P, García Nieto PJ, Castro-Fresno D. Comparative analysis of TIG welding distortions between austenitic and duplex stainless steels by FEM. *Applied Thermal Engineering*. 2010;30(16):2448-2459. <http://dx.doi.org/10.1016/j.applthermaleng.2010.06.016>.
- [17] Arunkumar M, Dhinakaran V, Sivashanmugam N, Petley V. Effect of plasma arc welding on residual stress and distortion of thin titanium sheet. *Materials Research*. 2020;22(6):e20190366. <http://dx.doi.org/10.1590/1980-5373-mr-2019-0366>.
- [18] Teng TL, Fung CP, Chang PH, Yang WC. Analysis of residual stresses and distortions in T-joint fillet welds. *International Journal of Pressure Vessels and Piping*. 2001;78(8):523-538. [http://dx.doi.org/10.1016/S0308-0161\(01\)00074-6](http://dx.doi.org/10.1016/S0308-0161(01)00074-6).
- [19] Gery D, Long H, Maropoulos P. Effects of welding speed, energy input and heat source distribution on temperature variations in butt joint welding. *Journal of Materials Processing Technology*. 2005;167(2-3):393-401. <http://dx.doi.org/10.1016/j.jmatprotec.2005.06.018>.
- [20] Pham X-T. Two-dimensional Rosenthal moving heat source analysis using the meshless element free Galerkin method. *Numerical Heat Transfer, Part A: Applications*. 2013;63(11):807-823. <http://dx.doi.org/10.1080/10407782.2013.757089>.
- [21] Dhinakaran V, Shanmugam NS, Sankaranarayanan K. Some studies on temperature field during plasma arc welding of thin titanium alloy sheets using parabolic Gaussian heat source model. *Proceedings of the Institution of Mechanical Engineers. Part C, Journal of Mechanical Engineering Science*. 2017;231(4):695-711. <http://dx.doi.org/10.1177/0954406215623574>.
- [22] Pilipenko A. *Computer simulation of residual stress and distortion of thick plates in multielectrode submerged arc welding: their mitigation techniques*. Trondheim: Norwegian University of Science and Technology; 2001
- [23] Radaj D. *Welding residual stresses and distortion: calculation and measurement*. 2nd ed. Düsseldorf: DVSVerlag GmbH; 2003. Modelling of welding residual stresses and distortion; p. 100-272.

